Title

Biogeochemical Anomalies at Two Southern California Current System Moorings During the 2014–2016 Warm Anomaly-El Niño Sequence

Journal

Journal of Geophysical Research - Oceans, 124(10)

ISSN

2169-9275

Authors

Lilly, Laura E
Send, Uwe
Lankhorst, Matthias
et al.

Publication Date

2019-10-01

DOI

10.1029/2019jc015255

Peer reviewed

JGR Oceans

RESEARCH ARTICLE
10.1029/2019JC015255

Biogeochemical Anomalies at Two Southern California Current System Moorings During the 2014–2016 Warm Anomaly-El Niño Sequence

Laura E. Lilly[1,2], Uwe Send[2,3], Matthias Lankhorst[3], Todd R. Martz[2,4], Richard A. Feely[5], Adrienne J. Sutton[5], and Mark D. Ohman[1,2]

[1]Integrative Oceanography Division, Scripps Institution of Oceanography, University of California, San Diego, La Jolla, CA, USA, [2]California Current Ecosystem Long-Term Ecological Research site, Scripps Institution of Oceanography, University of California, San Diego, La Jolla, CA, USA, [3]Climate, Atmospheric Sciences, and Physical Oceanography, Scripps Institution of Oceanography, University of California, San Diego, La Jolla, CA, USA, [4]Geosciences Research Division, Scripps Institution of Oceanography, University of California, San Diego, La Jolla, CA, USA, [5]NOAA Pacific Marine Environmental Laboratory, Seattle, WA, USA

Abstract We analyzed impacts of the 2014–2015 Pacific Warm Anomaly and 2015–2016 El Niño on physical and biogeochemical variables at two southern California Current System moorings (CCE2, nearshore upwelling off Point Conception; CCE1, offshore California Current). Nitrate and Chl-*a* fluorescence were <1 μM and <1 Standardized Fluorescence Unit, respectively, at CCE2 for the entire durations of the Warm Anomaly and El Niño, the two longest periods of such low values in our time series. Negative nitrate and Chl-*a* anomalies at CCE2 were interrupted briefly by upwelling conditions in spring 2015. Near-surface temperature anomalies appeared simultaneously at both moorings in spring 2014, indicating region-wide onset of Warm Anomaly temperatures, although sustained negative nitrate and Chl-*a* anomalies only occurred offshore at CCE1 during El Niño (summer 2015 to spring 2016). Warm Anomaly temperature changes were expressed more strongly in near-surface (<40 m) than subsurface (75 m) waters at both moorings, while El Niño produced comparable temperature anomalies at near-surface and subsurface depths. Nearshore $\Omega_{aragonite}$ at 76 m showed notably fewer undersaturation events during both warm periods, suggesting an environment more conducive to calcifying organisms. Planktonic calcifying molluscs (pteropods and heteropods) increased markedly in springs 2014 and 2016 and remained modestly elevated in spring 2015. Moorings provide high-frequency measurements essential for resolving the onset timing of anomalous conditions and frequency and duration of short-term (days-to-weeks) perturbations (reduced nitrate and aragonite undersaturation events) that can affect marine organisms.

Plain Language Summary The 2014–2016 Pacific Warm Anomaly-El Niño sequence significantly changed ocean conditions in the California Current System, but impacts of these anomalies on nutrients, chlorophyll-*a*, and pH, and comparisons to past El Niño events, have not been well described. We examined 9 years (2010–2018) of data from two ocean moorings that provide hourly measurements at fixed locations in the southern California Current System, allowing us to determine both subseasonal and multiyear ecosystem changes. We found that nitrate (important for primary production) and chlorophyll-*a* were anomalously low in nearshore waters throughout the Warm Anomaly and El Niño, suggesting nutrient delivery to the surface ocean was reduced. The Warm Anomaly and El Niño both produced anomalously warm shallow temperatures, but only El Niño produced significantly warmer waters below 50-m depth. Aragonite, a carbonate mineral important for shell production in calcifying marine organisms, showed elevated saturation state during both the Warm Anomaly and El Niño, suggesting the two anomalous periods produced favorable calcification conditions. Planktonic shelled molluscs, a key component of the oceanic food web, increased during both the Warm Anomaly and El Niño. Our findings may help predict impacts of future anomalies on nutrient availability and biological responses in the California Current System.

Key Points:
- Nearshore nitrate and Chl-*a* fluorescence were near zero for most of the Warm Anomaly-El Niño but increased briefly in spring 2015
- Temperature increases were surface-intensified across the region during the Warm Anomaly, while El Niño also affected subsurface waters
- Planktonic mollusc biomass was elevated in springs 2014 and 2016 in conjunction with Warm Anomaly and El Niño aragonite supersaturation

Supporting Information:
- Supporting Information S1

Correspondence to:
L. E. Lilly,
l1lilly@ucsd.edu

Citation:
Lilly, L. E., Send, U., Lankhorst, M., Martz, T. R., Feely, R. A., Sutton, A. J., & Ohman, M. D. (2019). Biogeochemical anomalies at two southern California Current System moorings during the 2014–2016 Warm Anomaly-El Niño sequence. *Journal of Geophysical Research: Oceans*, *124*, 6886–6903. https://doi.org/10.1029/2019JC015255

Received 1 MAY 2019
Accepted 30 AUG 2019
Accepted article online 6 SEP 2019
Published online 16 OCT 2019

1. Introduction

The California Current System (CCS) is an eastern boundary upwelling system that supports high biological production and commercially valuable fisheries. The southern portion of the CCS extends from Point Conception, CA, south to the U.S.-Mexico border and consists of the southward-flowing core California Current (200–400 km offshore), the nearshore poleward California Undercurrent (inshore of 150 km, centered at 150-m depth), and the Inshore Countercurrent (Di Lorenzo, 2003; Lynn & Simpson, 1987; Rudnick et al., 2017). The nearshore region experiences a spring upwelling season driven by alongshore winds, while wind-stress curl upwelling produces vertical pumping farther offshore; these dynamics deliver nutrients to near-surface waters, sustaining high primary production (Carr & Kearns, 2003; Chelton, 1982; Chelton et al., 1982; Cushing, 1971; Pickett & Paduan, 2003; Rykaczewski & Checkley, 2008). El Niño is the dominant mode of interannual variability in the CCS and can produce anomalous circulation including advection of water masses into the southern CCS from Baja California or southern offshore waters (Chavez, 1996; Chavez et al., 2002; Jacox et al., 2016; Lynn & Bograd, 2002; Simpson, 1984). El Niño impacts on CCS ecosystems vary substantially, but past major El Niños reduced phytoplankton biomass (Chavez, 1996; Fiedler, 1984; Kahru & Mitchell, 2000), produced anomalous subtropical zooplankton influxes (Bednaršek et al., 2018; Lavaniegos et al., 2002; Lavaniegos & Ohman, 2007; Lilly & Ohman, 2018; Rebstock, 2001), and altered survival and spatial distributions of seabirds and marine mammals (Keiper et al., 2005; D. E. Lee et al., 2007; Thayer & Sydeman, 2007).

The CCS can be affected by other modes of variability, including the Pacific Decadal Oscillation, the North Pacific Gyre Oscillation, and regionally forced non-Niño warm events (Di Lorenzo et al., 2008; Fiedler & Mantua, 2017; Mantua et al., 1997). The 2014–2015 Pacific Warm Anomaly that developed in the Eastern North Pacific Ocean showed unprecedented magnitude, spatial extent, and duration (Bond et al., 2015; Di Lorenzo & Mantua, 2016; Zaba & Rudnick, 2016). Anomalous sea surface temperatures (SSTs) appeared off California in spring 2014 and reached +5 °C in the upper 50 m of the water column (Gentemann et al., 2017; Zaba & Rudnick, 2016). The Warm Anomaly was associated with an "aborted El Niño" and was thus not attributed to direct equatorial El Niño forcing (Hu & Fedorov, 2016; Li et al., 2015), although atmospheric teleconnections from the equatorial Pacific likely influenced temperature anomalies in winter 2014–2015 (Chao et al., 2017; Di Lorenzo & Mantua, 2016). The Warm Anomaly persisted through spring 2015, at which point normal upwelling conditions produced cooler temperatures and high nutrients nearshore. Warm temperatures reappeared in summer 2015, and El Niño conditions reached the CCS by fall 2015 (Chao et al., 2017; Jacox et al., 2016). The sequence of the 2014–2015 Warm Anomaly followed immediately by the 2015–2016 El Niño produced more than 2 years of anomalous physical oceanographic conditions in the CCS, notably extremely warm temperatures and increased water column stratification (Jacox et al., 2016; Zaba & Rudnick, 2016). Despite known differences in physical forcing mechanisms, the Warm Anomaly had coastwide impacts on CCS ecosystems similar to those observed during El Niño events, including anomalously deep chlorophyll maxima (Zaba & Rudnick, 2016), subtropical zooplankton species appearances and community composition rearrangements (Fisher et al., 2015; Lilly & Ohman, 2018; Peterson et al., 2017), coastwide harmful algal blooms and associated marine mammal toxicity (McCabe et al., 2016; Ryan et al., 2017), and large-scale seabird mortality events (Peterson et al., 2015).

Ocean acidification is a growing issue due to increased anthropogenic release of CO_2 and subsequent oceanic uptake. The CCS experiences natural intrusions of low-pH, high-CO_2 conditions from upwelling of deep, remineralized waters, although these intrusions are predicted to expand and intensify in the future (Feely et al., 2008; Feely et al., 2016; Feely et al., 2018; Gruber et al., 2012; Hauri et al., 2013; Hauri et al., 2013; Leinweber & Gruber, 2013). Ocean acidification threatens calcifying marine organisms because it lowers the saturation states (Ω) of aragonite and calcite, carbonate minerals essential for shell production, requiring organisms to expend more energy on shell formation and growth (Bednaršek et al., 2014; Bednaršek et al., 2016; Bednaršek et al., 2017; Hauri, Gruber, McDonnell, & Vogt, 2013). Bednaršek et al. (2018) found that the pteropod species *Limacina helicina* in the northern CCS (southern British Columbia to Monterey Bay, CA) experienced synergistic negative impacts from an enhanced upwelling season (low oxygen, pH, and Ω_{arag}) in spring 2016 combined with increased temperatures during the 2013–2015 marine heat wave (here referred to as the Warm Anomaly) and

2015–2016 El Niño. Analysis of anomalous perturbations to CCS ecosystems and predictions of future impacts must therefore consider not just the event at hand but also its potential combination with background conditions and other perturbations.

Moorings provide continuous high-frequency measurements of a specific region and thus can resolve the onset timing of perturbations such as the Warm Anomaly and El Niño. They also provide information on short-term (days to weeks) habitat changes that organisms experience, such as pulsed nutrient delivery (Chavez, 1996; Chavez et al., 1997; Pennington & Chavez, 2000; Sakamoto et al., 2017) and aragonite undersaturation events. The present paper analyzes impacts of the 2014–2015 Pacific Warm Anomaly and 2015–2016 El Niño on subseasonal and interannual changes in multiple physical and biogeochemical variables measured at two southern CCS moorings that have been deployed regularly since January 2010. We specifically examined the following questions: (1) Did the 2014–2015 Warm Anomaly and 2015–2016 El Niño differentially affect physical and biogeochemical conditions in the southern CCS region? (2) Were the timing and magnitude of each event synchronous across CCE2 and CCE1? (3) Did the prior existence of the Warm Anomaly appear to influence subsequent biological responses to the 2015–2016 El Niño or long-term effects beyond the events? (4) How did biogeochemical responses to these two perturbations compare to the 2009–2010 El Niño?

We hypothesized that near-surface temperatures would be anomalously high and nitrate and chlorophyll-*a* fluorescence anomalously low at both moorings for the entire Warm Anomaly-El Niño sequence (spring 2014 to spring 2016). In contrast, we expected that deeper temperature anomalies would only appear during El Niño, and more strongly at CCE2 than at CCE1, due to coastally enhanced northward propagation of the El Niño signal. We further hypothesized that aragonite saturation state would be elevated at both moorings from spring 2014 to spring 2016, with corresponding increases in pelagic mollusc populations due to either advection of subtropical species or favorable in situ conditions.

2. Materials and Methods

2.1. Mooring Locations

Physical and biogeochemical data are from two biogeochemical moorings located in the southern CCS: CCE1 is located 220 km southwest of Point Conception, CA, in 4,100 m of water in the core southward-flowing California Current; CCE2 is located 35 km southwest of Point Conception in 800 m of water in the nearshore upwelling region (Figure 1). CCE1 is colocated with California Cooperative Oceanic Fisheries Investigations (CalCOFI) Station 80.80 and CCE2 with CalCOFI 80.55 (Bograd et al., 2003). CCE1 was initiated in October 2008 and CCE2 in January 2010, although both time series have experienced short-term interruptions. We present data here only from January 2010 to present. The moorings are maintained by the Ocean Time Series Group and the California Current Ecosystem Long-Term Ecological Research site, both based at Scripps Institution of Oceanography, La Jolla, CA.

2.2. Mooring Design and Sensors

Each mooring consists of a surface buoy with a buoy-mounted instrument package, including a Moored Autonomous pCO_2 sensor which measures seawater and air mole fractions of CO_2 (xCO_2) to be converted to partial pressure (pCO_2). A conductive wire connects subsurface instruments to the surface to permit real-time data transmission. Each mooring has a subsurface biogeochemical sensor cage: CCE1 at 40-m depth and CCE2 at 16-m depth. The cages include the following sensors: SBE37-IM Microcat (temperature and salinity), SeapHOx (pH sensor, Martz Lab, Scripps Institution of Oceanography) with attached Aanderaa optode (oxygen), WET Labs FLNTUS fluorometer (chlorophyll-*a* fluorescence), and Satlantic SUNA (nitrate). In addition to data from the sensor cages, we analyzed temperature and oxygen data at CCE2 at 76-m depth to calculate deep aragonite saturation (see section 2.4) and temperature and salinity data at CCE1 at 19 and 75 m to compare onset timing of the Warm Anomaly and El Niño between CCE1 and CCE2. Most of the sensors record data every 30 min; for the present study, we averaged data to daily values as described below. A detailed description of mooring design is available online (http://mooring.ucsd.edu/projects).

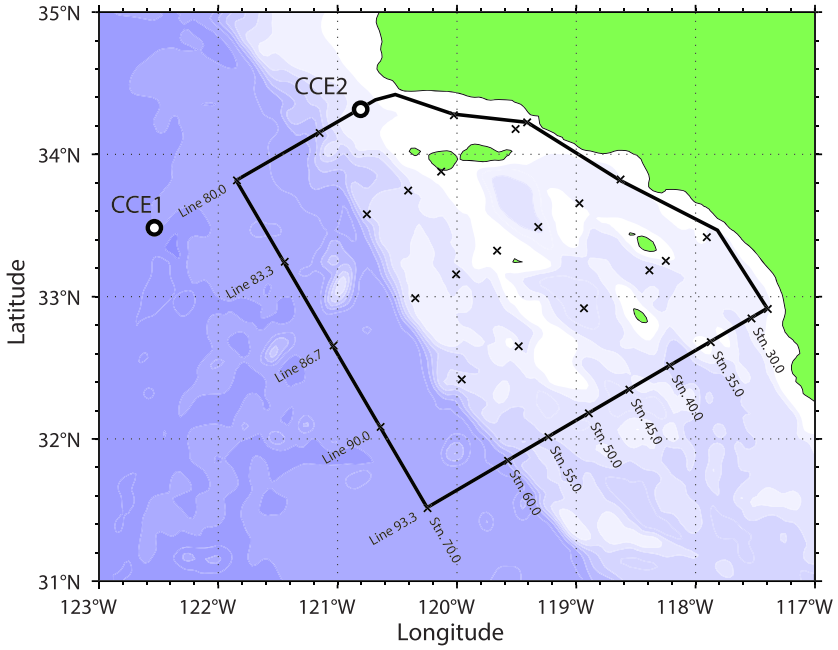

Figure 1. Locations of the CCE1 and CCE2 moorings (black circles) and subset of the California Cooperative Oceanic Fisheries Investigations (CalCOFI) sampling region from which zooplankton were analyzed (black box) in the southern California Current System. The CalCOFI stations from which zooplankton samples are pooled are shown by black crosses within and along the black box. Note that these stations are only a subset of the larger CalCOFI grid.

2.3. Sensor Calibrations and Quality Control

Microcat and optode sensors are calibrated by attaching sensors to a conductivity-temperature-depth rosette and conducting predeployment and postrecovery calibration casts to compare sensors to concurrent conductivity-temperature-depth measurements and bottle samples. Nitrate data undergo a two-step quality control process: (1) manual baseline correction to zero data and account for sensor drift and (2) comparison to in situ bottle-sample nitrate measurements for further correction. Chl-*a* fluorescence data undergo a three-step conversion process: (1) manual baseline correction, (2) conversion to Standardized Fluorescence Units (SFUs; cf. Powell & Ohman, 2015) by multiplying the raw time series by a slope value calculated by comparing fluorometer voltage readings to laboratory-prepared chlorophyll-*a* standards, and (3) comparison to CalCOFI Chl-*a* measurements for external validation and adjustment (see Appendix A and Figure A1 for additional information). The pH time series are quality controlled following Bresnahan et al. (2014) by bringing the subsurface SeapHOx pH sensors into agreement with a calculated surface reference pH at a time when the mixed layer is sufficiently deep to encompass the subsurface sensor. The surface reference pH is calculated from surface-measured pCO_2 data and total alkalinity estimated from temperature and salinity by the proxy relationships described in Alin et al. (2012). pCO_2 is measured as follows from Sutton et al. (2014): Mole fraction of CO_2 (xCO_2) in seawater is measured by pumping a sample of air through seawater for 10 min and then reading the equilibrated air sample using a LI-COR LI-820 CO_2 gas analyzer. A separate air sample is drawn into the Moored Autonomous pCO_2 sensor, and air xCO_2 is measured by the gas analyzer. Seawater and air measurements are made every 3 hr and calibrated in situ with a standard CO_2 reference gas. Raw (wet) xCO_2 measurements are converted to (dry) xCO_2 using atmospheric pressure and LI-820 vapor pressure, and dry measurements are used to calculate seawater and air pCO_2. $\Delta pCO_2 = pCO_{2SW} - pCO_{2air}$.

We averaged each time series to daily resolution to produce consistency across time series. Chl-*a* fluorescence daily values were only averaged from nighttime data points (2100–0300 local time) to avoid daylight quenching. Anomalies were computed by removing the 2010–2018 mean for each year-day from the corresponding year-day for each year (e.g., 1 January of each year minus the 1 January 2010–2018 mean). We compared time series to quarterly CalCOFI cruise measurements at the appropriate station and depth as an external data check for all time series except pH and pCO_2 (CalCOFI data not available; Figures 2 and 4),

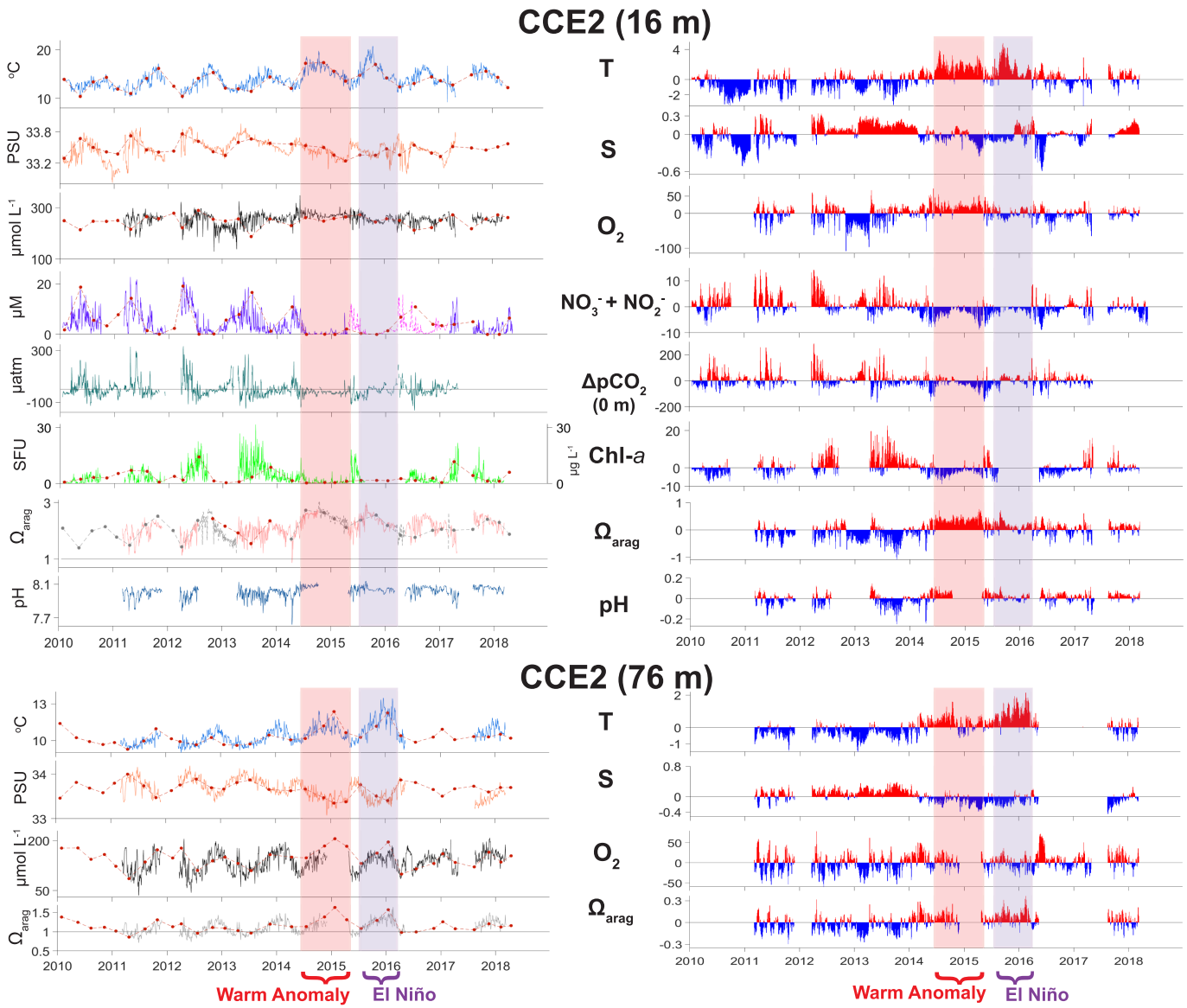

Figure 2. Daily-averaged time series (left) and anomalies (right) for the CCE2 mooring at 16 m (top) and 76 m (bottom). Variables at 16 m are (top-bottom) temperature, salinity, oxygen, nitrate+nitrite, ΔpCO_2, Chl-*a* fluorescence (SFU), omega-aragonite, and pH. Horizontal gray lines for Ω_{arag} at 16 and 76 m indicate the aragonite saturation horizon ($\Omega = 1$); undersaturation events occur when the time series dips below this line. The nitrate time series at 16 m includes measured data (purple) and temperature-proxy calculations (magenta). Aragonite saturation time series at 16 and 76 m include proxy calculations from pH-CO_2 (light pink, 16 m only) and temperature-O_2 (gray, 16 and 76 m; see section 2.4 and Appendices A and B for nitrate and aragonite saturation calculations). The Warm Anomaly and El Niño are shaded by vertical orange and purple bars, respectively. Red dots and dashed lines on left panels are California Cooperative Oceanic Fisheries Investigations quarterly measurements (not available for pCO_2 or pH; Chl-*a* scale as µg/L, right axis).

although these types of pH and pCO_2 checks have been performed as part of previous studies (Sutton et al., 2014; Sutton et al., 2016). The carbonate chemistry calculations described in this section and the following section were carried out using CO2SYS for Matlab v1.1 (Van Heuven et al., 2011).

2.4. Aragonite Saturation State Calculations

Aragonite saturation state (Ω_{arag}) was calculated using two approaches. The first estimates Ω_{arag} from measured pH and estimated total alkalinity calculated from the proxy mentioned in section 2.3. We applied this approach using the pH sensor data at CCE1 40 m and CCE2 16 m. We used a second proxy relationship to

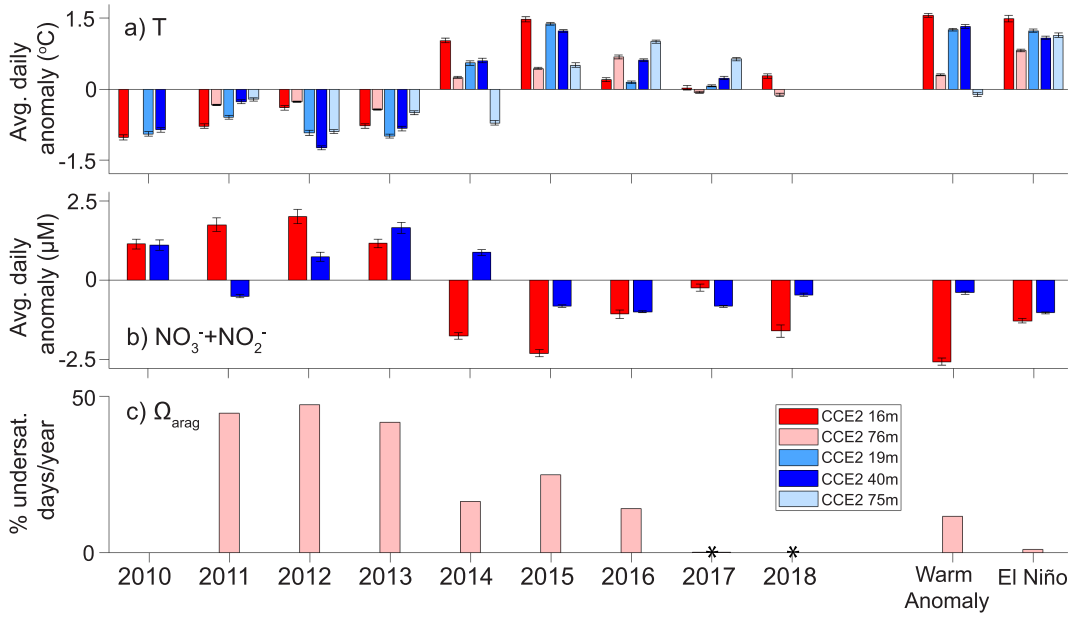

Figure 3. Average daily anomalies for (a) temperature and (b) nitrate+nitrite, both at several depths at CCE1 and CCE2. (c) Percent of aragonite undersaturation days per year at CCE2 at 76 m. Average daily anomalies and percentages are calculated for each yearlong period (1 January to 31 December) and the Warm Anomaly and El Niño (see Appendix C for anomaly start and end dates). Error bars are standard error. Legend in (c) refers to all panels. Asterisk (*) symbols in (c) indicate years of insufficient data for calculations.

calculate Ω_{arag} at CCE2 76 m using temperature and oxygen, as described in Alin et al. (2012). The relationship between Ω_{arag} and temperature-O_2 holds beneath the mixed layer but is often also valid at shallower depths in upwelling areas such as CCE2. Due to the high correlation between the pH-derived Ω_{arag} and temperature-O_2 proxy at CCE2 16 m (rho = 0.90, $p < 0.01$), we supplemented the pH-derived Ω_{arag} calculations at CCE1 40 m and CCE2 16 m with calculations from the second relationship during periods for which we lacked pH data (see Appendix B for more information). For comparison, we also calculated Ω_{arag} from quarterly CalCOFI bottle data corresponding to CCE1 40 m, CCE2 16 m, and CCE2 76 m. We used dissolved inorganic carbon and total alkalinity measurements at CCE1 40 m and CCE2 16 m from the five cruises for which they are available (pH data are not available from CalCOFI cruises). For other cruises and all calculations at CCE2 76 m, we calculated CalCOFI Ω_{arag} from temperature and oxygen.

To estimate the percentage of aragonite undersaturation days in a year, we summed the number of days of aragonite undersaturation within a yearlong period (1 January to 31 December) or the Warm Anomaly or El Niño and divided by the number of sampled days of aragonite saturation in that period (see Appendix C for start and end date of each anomalous period). The resulting values for "% aragonite undersaturation days/year" are shown in Figure 3c.

2.5. Temperature and Nitrate Cumulative Anomalies

We demarcated the start and end dates of the Warm Anomaly and El Niño as the beginnings and ends of periods of continuous positive temperature anomalies during spring 2014 to spring 2016 at the near-surface sensors (16 m for CCE2 and 19 m for CCE1; see Appendix C for explanation and dates). The resulting periods are shaded in Figures 2 and 4. We calculated average daily anomalies for temperature and nitrate during the Warm Anomaly and El Niño to compare the individual impacts of each perturbation and their differential effects in near-surface and subsurface waters. We used the temperature-derived start and end dates for nitrate anomaly calculations to maintain consistency and because nitrate did not have continuous negative anomalies throughout each perturbation. For each anomalous period, we summed all temperature or nitrate anomalies at a given depth to obtain the total integrated anomaly for that depth, which we then divided by the total number of perturbation days to get the average daily anomaly.

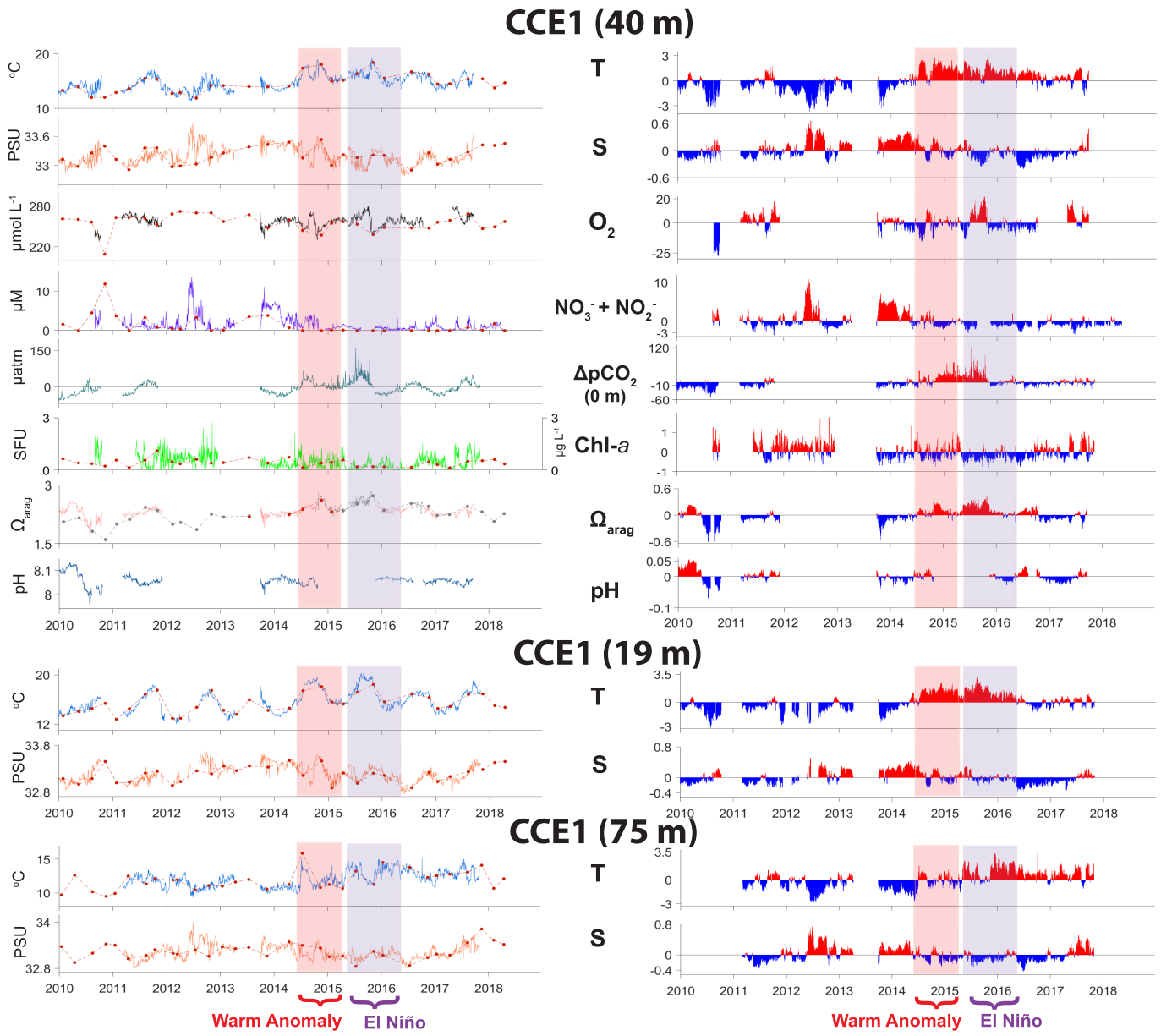

Figure 4. As in Figure 2 but for CCE1 sensors at 40 m (top row), 19 m (middle row), and 75 m (bottom row). Only temperature and salinity are shown for 19 and 75 m.

2.6. North/South Water Mass Index and Particle Backtracking

An index of the relative contributions of northern- versus southern-origin flow (hereafter: N/S index) was previously developed to identify origins of water masses arriving at the CCE1 mooring, based on temperature-salinity (T-S) properties. The N/S index was developed from temperature and salinity data from locations in the CCS between Northern California and the southern tip of Baja California using data from the World Ocean Atlas climatologies (Locarnini et al., 2013; Zweng et al., 2013). Locations were assigned N/S index values on a scale from −1 (Northern California) to +1 (southern Baja California) based on where their T-S diagrams fit in relation to the southernmost and northernmost water masses. The CCE1 N/S index at 40 m was then computed by determining where its combined T-S values aligned with the standardized values from −1 to +1. Our N/S index is akin to the spiciness property (Flament, 2002) or to analyzing salinity on a fixed isopycnal, but the −1 to +1 scaling adjusts the values to the local hydrography. Waters at CCE1 with positive N/S index values suggest southern or offshore origins.

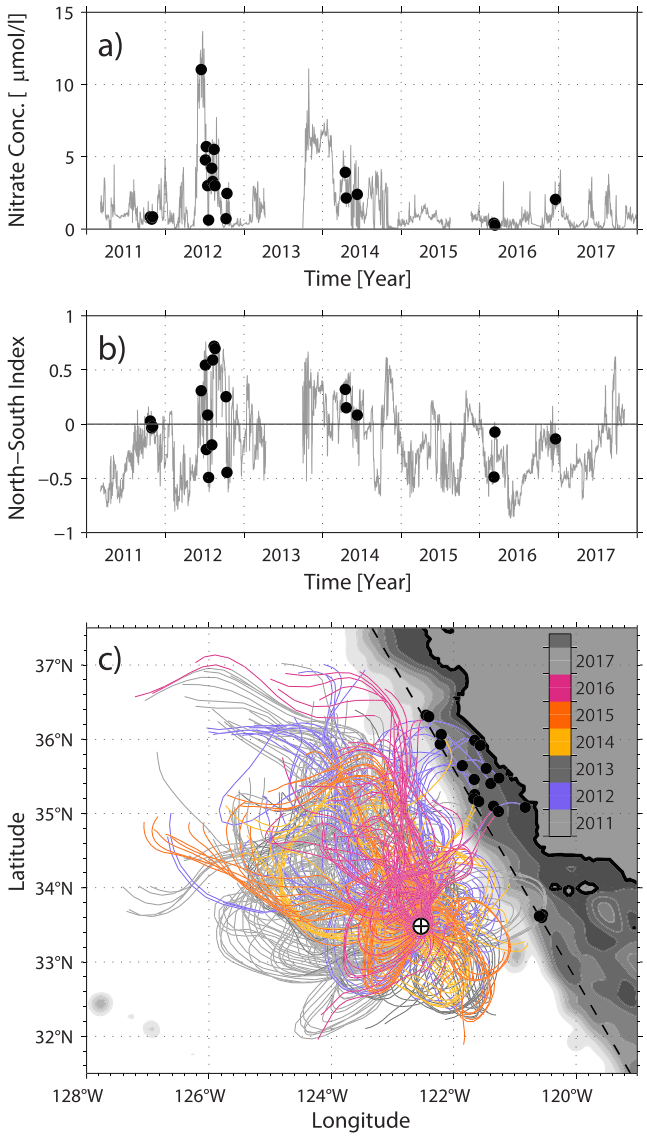

Figure 5. Comparison of (a) nitrate at CCE1 at 40 m and (b) North/South index of water mass origin for waters arriving at CCE1. Positive values indicate southern-origin waters. (c) Surface particle trajectories based on altimetry-derived geostrophic velocities. The velocity fields were integrated to find trajectories that end at the CCE1 site (marked). Each trajectory is 30 days in duration (trajectories are shown for every 30-day period of each year). Trajectories with prior excursions in nearshore waters (east of the dashed line) are marked by black dots. Matching black dots in (a) and (b) show the arrival times of these nearshore trajectories to CCE1. See Figure S1 for particle tracks by individual year.

The CCE1 site is located in the climatological mean position of the California Current, but as the current meanders back and forth, inflow to CCE1 can occur from different directions (see also figure 11 in Frischknecht et al., 2018). To investigate whether southern-appearance waters at CCE1 indicated by the N/S index were associated with southern- or coastal-origin flows, we analyzed surface particle trajectories. These were computed from altimetry-derived geostrophic currents, which are distributed as part of the Copernicus Marine Environment Monitoring System (formerly AVISO). From these currents, we computed particle trajectories by solving the equation $\vec{u} = \frac{d\vec{X}}{dt}$, where $\vec{u}$ denotes the Eulerian velocities from the altimeter and $\vec{X}$ denotes the Lagrangian positions along a trajectory. We integrated the resulting velocities backward for 30 days prior to the CCE1 endpoint. Each particle track starts 5 days after the previous track starts, so successive tracks overlap for 25 days; there are 533 tracks total for the entire period from 2010 to 2018. We compared our altimetry-derived particle trajectories to acoustic Doppler current profiler (ADCP)-derived trajectories from CCE1 at 30-m depth and found strong correspondence for the 30-day forward projections (see Appendix D and Figure D1 for more information). Prior results from Hartman et al. (2010); see their figure 5) also suggest that qualitative comparisons using these trajectories are reasonable. We did not calculate particle trajectories for CCE2 (located 35 km from land) because altimetry data within 50 km of the coast are generally unreliable and would likely not produce accurate backtracks.

2.7. Pelagic Mollusc Sampling

Zooplankton were collected on CalCOFI cruises as previously described (Lavaniegos & Ohman, 2007; Lilly & Ohman, 2018). Samples were collected by a 505-µm mesh, dual-opening, 0.71-m diameter bongo net towed obliquely from 0 to 210 m. After collection, samples were preserved in formaldehyde buffered with sodium tetraborate and then archived for identification in the Pelagic Invertebrate Collection at Scripps Institution of Oceanography. All nighttime stations within the Southern California region (CalCOFI Lines 80–93.3 from the coast to Station 70, excluding stations <200-m depth) were pooled into one aliquot per cruise. Pelagic molluscs (i.e., thecosome and gymnosome pteropods and heteropods) from spring cruises only were identified to genus (where possible) or higher taxon using light microscopy. Within the total pelagic mollusc group, we also present data for the family Limacinidae and for *Hyalocylis* spp., which only appeared in 2014 and was comprised almost exclusively of *H. striata* (L. Sala, 15 Jun 2019). The family Limacinidae is not enumerated to species level but is likely comprised of the following six species based on past descriptions of pteropod biogeographies in the eastern North Pacific: *Heliconoides inflatus*, *Limacina helicina helicina*, *L. helicina pacifica*, *L. bulimoides*, *L. lesueruii*, and *L. trochiformis* (Janssen et al., 2019; McGowan, 1967).

3. Results and Discussion

3.1. The 2014–2015 Warm Anomaly: Evolution and Effects

The 2014–2015 Pacific Warm Anomaly produced the longest period of consistently anomalously warm temperatures and near-zero nitrate and chlorophyll-*a* fluorescence at CCE2 since our mooring time series began

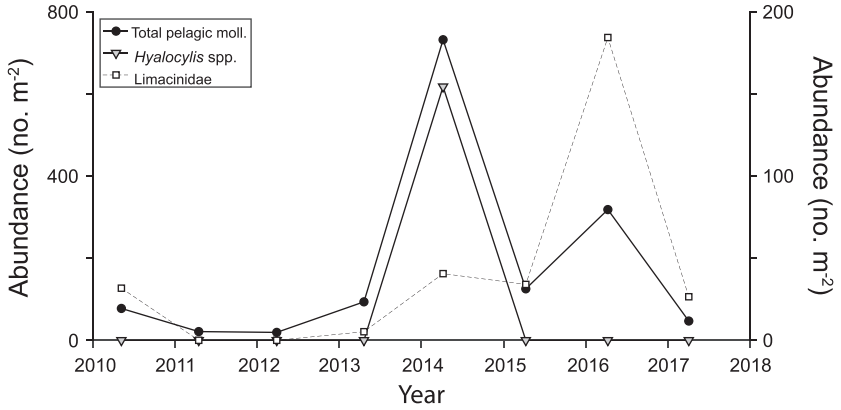

Figure 6. Abundance of total pelagic molluscs (solid dots and solid line), *Hyalocylis* spp. (gray triangles and solid line), and family Limacinidae (open squares and dashed line). Symbols represent spring cruise values. Total mollusc and *Hyalocylis* spp. values are shown on the left axis and family Limacinidae values are shown on the right axis.

(Figure 2). Nitrate levels were <1 μM and chlorophyll-*a* was <1 SFU for the entire period of May 2014 to February 2015. Average daily nitrate anomalies at CCE2 at 16 m during the Warm Anomaly were twice the (negative) magnitude of those during El Niño, suggesting that the Warm Anomaly more completely suppressed nitrate inputs to the nearshore region (Figure 3b, red bars). In contrast to CCE2, negative nitrate anomalies at CCE1 only appeared halfway through the Warm Anomaly, and Chl-*a* anomalies increased from moderately negative to positive despite decreasing nitrate levels (Figure 4).

The unusual high nitrate at CCE1 in spring–summer 2014 may have been due to horizontal offshore advection of nutrients from southern-origin waters. To analyze this possible source, we calculated a northern- versus southern-origin water mass index (N/S index), which scales the T-S properties of a given water mass from −1 (Northern California) to +1 (southern Baja California). At CCE1 at 40 m, the N/S index shows predominantly positive values during mid-2012 and 2013–2014, suggesting enhanced subtropical water mass delivery as a source of nitrate (Figures 5a and 5b). We also computed 30-day backtracked surface water trajectories for particles arriving at CCE1, to further determine the origins of positive N/S index values. Trajectories show that water parcels arriving at CCE1 in mid-2012 and spring 2014 originated predominantly from the nearshore region (black dots in Figure 5; see supporting information Figure S1 for particle tracks separated by year). Particle tracks in mid-2012 show nearshore origins off central California (Figure 5c, purple lines; Figure S1 yellow-green lines), suggesting upwelled waters were transported to CCE1 by an offshore-moving filament that also increased nitrate and salinity at CCE2. In contrast, CCE1 tracks in winter 2013–2014 appeared to originate from southern waters offshore of the dotted line (Figure 5c; dark gray tracks indicate 2013 and yellow tracks 2014 in southern region; see Figure S1 for within-year seasonal timing). Subsequent minor nitrate inputs to CCE1 in spring 2014 appeared to come from nearshore (yellow tracks and black dots in Figure 5c), suggesting some cross-shore delivery to CCE1 at the beginning of the Warm Anomaly despite significantly reduced nitrate at CCE2.

Shallow temperature measurements at CCE2 at 16 m (Figure 2) and CCE1 at 19 and 40 m (Figure 4) indicate concurrent onset of continuous positive temperature anomalies across the region in June 2014. Our timing is consistent with satellite SST measurements by Gentemann et al. (2017), who found that anomalously warm SSTs appeared rapidly across the southern CCS region at the end of June 2014 and subsequently expanded north to connect with offshore North Pacific anomalies. Temperature measurements at CCE2 at 76 m show moderate positive anomalies during the Warm Anomaly but daily average anomalies only one fourth of near-surface anomalies, while temperatures at CCE1 at 75 m show slightly negative daily average anomalies during the Warm Anomaly (Figure 3a; CCE2—red vs. light pink bars; CCE1—pale blue bars). These findings are consistent with glider observations from Zaba and Rudnick (2016) that the Warm Anomaly was a surface-intensified (<75 m) phenomenon across the southern CCS.

Spring 2014 showed a 14-fold increase in total pelagic mollusc abundance compared to the 2010–2013 mean. The increase was predominantly driven by unusual presence of *Hyalocylis* spp., which were comprised in 2014 predominantly of the subtropical species *Hyalocylis striata* (Figure 6; L. Sala, personal

Table B1
Aragonite Undersaturation Day-Counts and Durations at CCE2 (76-m Depth)

Year	No. days $\Omega < 1$ (raw)	Consecutive days (events > 1 day)	Days of data	No. days $\Omega < 1$ (normalized to year-days)
2010	—	—	0	—
2011	119	6, 5, 20, 4, 21, 4, 30, 2, 8, 8, 4, 2, 3	267	0.446
2012	133	6, 12, 2, 13, 5, 37, 21, 28, 5, 3	282	0.472
2013	150	5, 38, 8, 27, 19, 2, 3, 9, 9, 6, 3, 4, 5, 4, 4	361	0.416
2014	52	3, 2, 4, 13, 15, 4, 8	317	0.164
2015	62	16, 42, 3	248	0.250
2016	19	14, 2, 2	134	0.142
2017	1	—	134	0.008
2018	0	—	73	0
Warm Anomaly	20	3, 4, 8, 4	173	0.116
El Niño	3	3	251	0.012

communication). Abundance of family Limacinidae was also moderately elevated in spring 2014. These increases coincided with the onset of elevated aragonite saturation (Ω_{arag}) and pH in spring 2014, likely due to reduced upwelling of high-CO_2, low-O_2 waters (Feely et al., 2008; Feely et al., 2016; Hauri, Gruber, McDonnell, & Vogt, 2013; Leinweber & Gruber, 2013; McLaughlin et al., 2018). Although our N/S index was developed to assess nutrient delivery, we can also use it as an approximate indicator of advection of southern-origin plankton. As noted above, the N/S index suggests enhanced presence of southern-origin waters in winter–spring 2014. In contrast, favorable aragonite conditions only appeared in spring 2014, coincident with, rather than preceding, increased pelagic mollusc abundance. We therefore conclude that the increase in mollusc abundance in spring 2014 is due to increased advection of subtropical populations into the region rather than in situ population growth.

Offshore elevated nitrate and the marked increase in subtropical molluscs in spring 2014 suggest that the southern CCS received a significant input of southern-origin waters at the beginning of the Warm Anomaly. Reduced nitrate at CCE2 during this period may be explained by subregional variations in forcing mechanisms. The nearshore region was characterized in spring 2014 by locally increased downward surface heat flux, reduced upwelling winds, high water column static stability, and anomalously deep thermocline, nutricline, and subsurface chlorophyll maximum layers (Bond et al., 2015; Zaba & Rudnick, 2016). A depressed nutricline and reduced vertical mixing would reduce nutrient delivery to surface waters despite possible continued nutrient advection at depth. We note the slightly negative nitrate and Chl-*a* anomalies at CCE2 in spring 2014 as further evidence for a moderately reduced upwelling season preceding region-wide onset of the Warm Anomaly. CCE1, located in the southward-flowing core California Current, measures an ocean environment forced predominantly by horizontal advection and some wind-stress-curl upwelling rather than wind-driven upwelling (Di Lorenzo, 2003; Rykaczewski & Checkley, 2008). Minor differences in response timing and magnitude at CCE1 and CCE2 suggest that some subregional nutrient delivery mechanisms acted on CCE1 at the start of the Warm Anomaly despite region-wide onset of temperature anomalies. Offshore nutrient delivery to CCE1 apparently decreased or reversed partway through the Warm Anomaly, however, as indicated by near-zero nitrate levels. These findings are consistent with observations by Zaba and Rudnick (2016) of onset of downwelling-related onshore flow in 2014–2015.

3.2. Spring 2015 Interlude and 2015–2016 El Niño Impacts

High nitrate and pCO_2 pulses, increased Chl-*a*, and anomalously cool temperatures at CCE2 were observed from March to June 2015, suggesting that a moderate nearshore upwelling season occurred between the Warm Anomaly and the start of El Niño (Figure 2). Offshore CCE1 temperature anomalies also decreased in spring 2015 but immediately returned to Warm Anomaly levels in summer 2015. Our findings of a direct transition from Warm Anomaly to El Niño temperature conditions offshore are consistent with other studies in the southern CCS and coastal Baja California regions and again highlight subregional differences in event forcing mechanisms (Gentemann et al., 2017; Robinson, 2016).

CCE2 temperature anomalies increased in fall 2015 and produced El Niño daily average values comparable to the Warm Anomaly (Figure 3a, red bars). Nitrate levels at CCE2 decreased in summer 2015 and remained low through the duration of El Niño, although daily average nitrate anomalies were smaller than during the

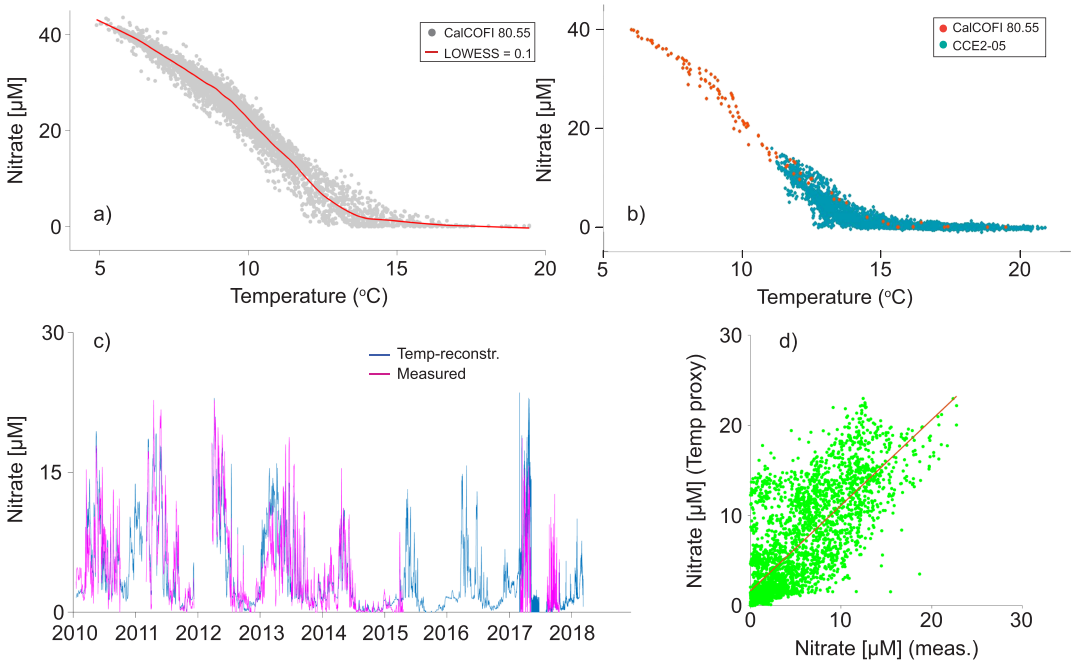

Figure A1. Temperature reconstruction of nitrate. (a) Temperature-nitrate relationship for all CalCOFI data collected at CCE2 (Station 80.55, 1951–2016), shown as gray dots. Red line is the LOWESS relationship for $f = 0.1$. (b) Temperature-nitrate relationship for CCE2-05 deployment data (turquoise dots) and corresponding CalCOFI data at Station 80.55 during the same time period (orange dots). (c) Time series comparison of CCE2 sensor-measured nitrate (pink line) versus temperature-reconstructed nitrate (blue line) for the entire CCE2 mooring time series. (d) Measured versus temperature-reconstructed nitrate from the data in c (rho = 0.77, $p < 0.01$). CalCOFI = California Cooperative Oceanic Fisheries Investigations; LOWESS = locally weighted scatterplot smoothing.

Warm Anomaly (Figure 3b, red bars). We do not have CCE2 Chl-*a* data during El Niño, but quarterly CalCOFI measurements indicate that Chl-*a* remained low from summer 2015 to fall 2016 despite moderate nitrate inputs in spring 2016. Sustained negative nitrate and Chl-*a* anomalies at CCE1 only occurred during El Niño, and daily average nitrate anomalies were greater than during the Warm Anomaly (Figure 3b, blue bars). Persistent low nitrate at CCE1 throughout El Niño is consistent with particle trajectories indicating water mass origins in 2015–2016 predominantly in the surrounding and offshore regions that had likely already undergone nutrient drawdown (Figure 5c, orange and magenta tracks).

Deeper (75–76 m) temperature anomalies at both moorings were comparable to near-surface values during El Niño, and daily average anomalies were 2–5 times greater than during the Warm Anomaly (Figure 3a, light pink and light blue bars). El Niño onset in the CCS was attributed partly to coastally trapped waves from the equatorial Pacific (Frischknecht et al., 2017), which may explain anomalous deep temperatures. However, thermocline depth and upwelling winds were anomalously shallow and strong, respectively, in fall–winter 2015–2016, more in line with normal CCS upwelling conditions than with past El Niños or the Warm Anomaly (Gentemann et al., 2017; Jacox et al., 2016). Shorter duration and smaller negative daily average nitrate anomalies at CCE2 during El Niño compared to the Warm Anomaly likely reflect this moderate upwelling response in fall–winter 2015–2016. Decreases in deep temperatures and aragonite saturation state in May 2016 indicate the abrupt end of the El Niño event, likely due to the appearance of moderate spring upwelling. However, Jacox et al. (2016) predicted that chlorophyll levels off central and southern California would remain low in spring 2016 due to the combined low-nutrient Warm Anomaly-El Niño period. Persistent low Chl-*a* at CCE2 in spring 2016 despite moderate nitrate inputs support this prediction and could reflect phytoplankton community changes or enhanced grazer control.

Total pelagic mollusc abundance declined slightly in spring 2015 relative to 2014 and 2016 but was still higher than other years. Population declines in 2015 may have occurred in response to aragonite undersaturation at CCE2 at 76 m (Figure 2; time series dips below horizontal gray line at $\Omega = 1$) or to cessation of

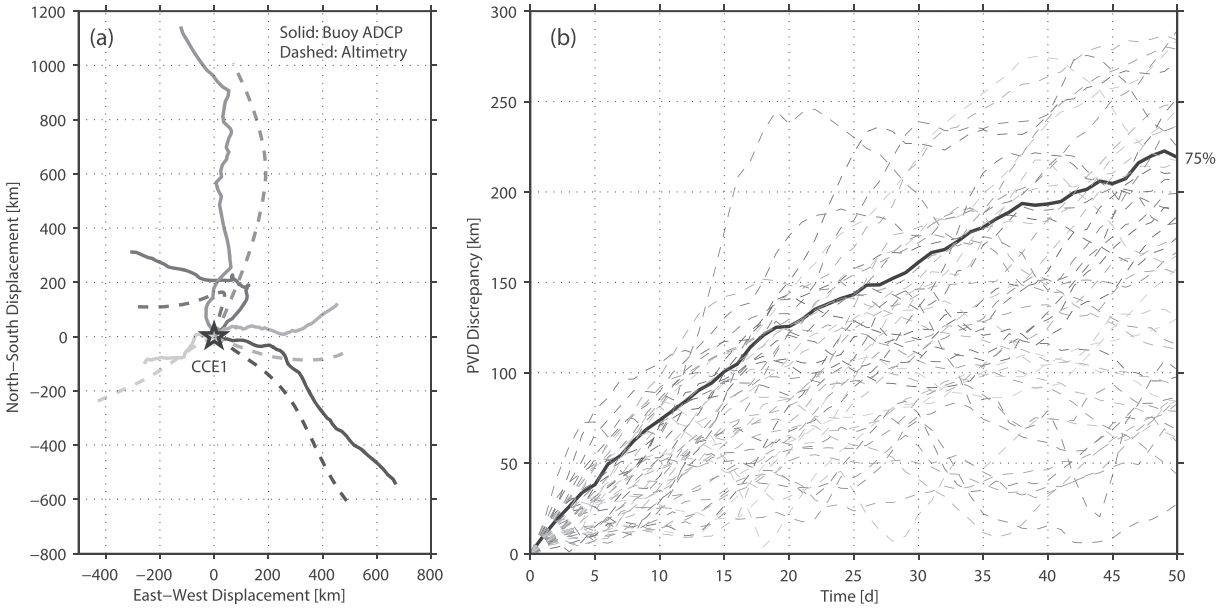

Figure D1. (a) Selection of 5 (out of 45) progressive vector diagrams computed by integrating observed in situ velocities from an ADCP (solid lines) and altimetry-derived velocities (dashed lines) at the CCE1 location forward for 30 days. (b) Discrepancies between each pair of ADCP-altimetry simulations. Thick black line shows 75th percentile. ADCP = acoustic Doppler current profiler.

anomalous advection. As noted above, our N/S index indicates northern- and within-region flows to CCE1 throughout 2015, suggesting lower subtropical influxes than in spring 2014 (Figure 5c). Elevated total mollusc abundance in 2015 above non-anomalous springs (2011–2013 and 2017) may indicate continued population persistence following 2014, particularly of family Limacinidae. This persistence was likely due to continued moderate in situ reproduction and individual growth. However, the spring 2015 decrease in abundance compared to 2014 and 2016 suggests that a period of separation occurred between the increases in springs 2014 and 2016. Total pelagic mollusc and Limacinidae abundances were again elevated in March–April 2016 (5 and 15 times higher, respectively, than their 2010–2013 means) toward the end of the El Niño event, although the subtropical species (*H. striata*) that dominated in spring 2014 was absent. The N/S index and particle tracks suggest lower southern-origin flow in winter–spring 2016 than in 2014, while aragonite saturation conditions remained favorable ($\Omega_{arag} > 1$). We therefore posit that increased mollusc abundances in spring 2016 were due to in situ growth of existing populations (either resident or seeded from the south in 2014) in response to elevated aragonite levels rather than to advection of new populations. Our spring 2016 samples likely captured the height of pelagic mollusc population growth before the return of moderate upwelling conditions and decreased aragonite levels in late spring 2016.

Bednaršek et al. (2018) showed negative pteropod responses in the northern CCS to the 2013–2016 combined marine heat wave, El Niño, and enhanced upwelling. Aguilera et al. (2019) similarly observed reductions in growth and egg production in the resident copepod *Acartia tonsa* in the Humboldt Current System under warm, acidic conditions in 2015. Our finding of increased pelagic molluscs in the southern CCS in springs 2014 and 2016 may be explained by several factors. First, subtropical pelagic molluscs were likely advected into the region in spring 2014 and would have contributed to the sudden population increase even if existing cooler-water species were thermally stressed. Subtropical species likely benefitted from warmer temperature conditions of the Warm Anomaly and El Niño and may have grown in situ beyond their initial advection, further offsetting decreases in cool-water species. Second, while the southern CCS experienced extreme positive temperature anomalies during 2014–2016, Ω_{arag}, pH, and oxygen were all elevated, producing calcifying-favorable conditions that perhaps ameliorated temperature stress. The longest periods of consecutive aragonite undersaturation in our records during the Warm Anomaly and El Niño were significantly shorter than in 2011–2013 (see Table B1 for values). Bednaršek et al. (2018) note that altered carbonate conditions have a dominant effect on pelagic mollusc health at the cellular level. The favorable carbonate conditions we observed likely provided some offset to thermal stress in 2014 and 2016, while moderate upwelling in

spring 2015 produced less favorable carbonate conditions and may have negatively impacted organisms despite cooler temperatures and increased food availability. Third, Bednaršek et al. (2016) note that euthecosome pteropods are omnivores, and many species feed using mucous nets. These feeding strategies may have allowed some molluscs to increase despite overall reduced primary production and smaller phytoplankton sizes during the Warm Anomaly and El Niño, perhaps also offsetting negative effects of thermal stress. Aguilera et al. (2019) observed that *A. tonsa* maintained normal body size despite unfavorable habitat conditions during both the 2015 warm period and general upwelling conditions. The authors attribute this to elevated phytoplankton prey, suggesting food availability may partially offset negative physical oceanographic conditions. Both Bednaršek et al. (2018) and our current study suggest that pelagic mollusc responses vary depending on specific combinations of favorable and unfavorable habitat changes. Subtropical-associated species appear to benefit from El Niño-induced combinations of increased northward advection and in situ elevated aragonite saturation in the southern CCS, conditions which allow them to temporarily expand their population ranges. Future El Niño-like perturbations therefore need to be evaluated for comprehensive changes in advection, temperature, aragonite, and food availability, in order to predict full effects on pelagic molluscs.

3.3. Comparison of 2014–2016 Warm Anomaly-El Niño Period to 2009–2010 El Niño

Our CCE2 time series measured the second half of the 2009–2010 El Niño, an event of known anomalous forcing in the CCS (Todd et al., 2011) which produced atypical zooplankton community changes relative to other El Niños (Lilly & Ohman, 2018). The 2009–2010 El Niño was characterized by direct atmospheric teleconnections from the tropical Pacific to the CCS, with resulting changes in local wind circulation and a lack of oceanic coastally trapped wave propagation (Todd et al., 2011). Nitrate and ΔpCO_2 at CCE2 were elevated in 2010 compared to the 2014–2016 period, although lower than 2011–2013, a period encompassing a moderate La Niña and productive CCS conditions (Bjorkstedt et al., 2012; Wells et al., 2013). However, Chl-*a* at CCE2 was anomalously low in 2010, comparable to post-El Niño levels in spring 2016. We have minimal nitrate, ΔpCO_2, and Chl-*a* data at CCE1 from 2010, but CalCOFI measurements suggest that all three variables were slightly elevated in winter–spring 2010 compared to the 2015–2016 El Niño, indicating a more minimal offshore impact of the 2009–2010 El Niño. Biomass of pelagic molluscs, notably the pteropod family Limacinidae, was also moderately elevated in spring 2010 in conjunction with positive Ω_{arag} anomalies at CCE1 and CCE2. Although the 2009–2010 El Niño impacts in the CCS have been attributed to atmospherically forced local physical changes rather than direct oceanic propagation, the perturbation still produced low Chl-*a* and favorable calcifying conditions at both moorings.

4. Conclusions

Temperature data suggest that the 2014–2015 Pacific Warm Anomaly developed rapidly region-wide in the southern CCS in spring 2014, although nutrient delivery appeared to show subregional differences between offshore and nearshore regions. Coastal waters experienced rapid and sustained onset of upwelling suppression, with likely negative consequences for primary production. Our observations of surface-intensified temperature anomalies during the Warm Anomaly confirm other evidence for a combination of thermocline depression, increased stratification, and reduced wind stress as a cause of reduced upwelling (Zaba & Rudnick, 2016). In contrast, from the outset, the 2015–2016 El Niño was expressed in subsurface (75 m) as well as surface waters. Offshore nutrient anomalies were much more pronounced during El Niño than during the Warm Anomaly. Neither the Warm Anomaly nor El Niño individually, nor their multiyear combination, appeared to have residual negative impacts on chlorophyll concentration, as evidenced by moderately elevated nitrate and Chl-*a* in 2017–2018.

The elevated abundance of pelagic molluscs during both the Warm Anomaly and El Niño suggests that some organisms may have benefited from these anomalous conditions. While increased pelagic mollusc abundances in spring 2014 were likely due partly to increased northward advection of subtropical species, recurrences in spring 2016 appeared more attributable to in situ growth. Aragonite undersaturation events in the CCS are expected to increase spatially and temporally in the future due to the ocean's absorption of anthropogenic CO_2 (Feely et al., 2008; Feely et al., 2016; Hauri, Gruber, McDonnell, & Vogt, 2013). More frequent and longer-duration aragonite undersaturation events can have significant negative impacts on calcifying organisms, including reduced growth, shell dissolution, and decreased survival (Bednaršek et al., 2014;

Osborne et al., 2016). However, El Niño events are also predicted to become more extreme in future decades (Cai et al., 2014; T. Lee & McPhaden, 2010), and such events might create short-term suitable habitat for subtropical calcifiers to increase. We note that northward displacements of subtropical species may temporarily reduce their abundances in their original habitats, but we do not presently know what impacts such biogeographic shifts may have on the original community. Continued high-frequency biogeochemical measurements should be combined with species-level analysis of pelagic mollusc communities to develop a framework for predicting how zooplankton populations in Eastern Boundary Upwelling Systems will vary both short- and long-term in response to ocean changes.

Appendix A: Nitrate and Chl-*a* Fluorescence Sensor Calibrations and Quality Control

Nitrate quality control steps are as follows: First, the raw SUNA data are plotted, and a smooth zero baseline is drawn along the lower edge of the time series and subtracted from the raw data to obtain baseline-corrected data. This baseline is often nonlinear and nonmonotonic and removes sensor drift and zero offset. Second, the baseline-corrected time series is compared to in situ nitrate measurements (pre-mooring and post-mooring deployment calibration casts and quarterly CalCOFI nitrate measurements) to check sensor accuracy. Additional baseline offset is applied as needed to match the sensor time series to calibration measurements.

Three mooring deployments (CCE1: September 2012 to May 2013; CCE2: April 2015 to May 2016 and May 2016 to March 2017) had SUNA sensor failure, so those time series were reconstructed using a temperature-nitrate proxy. Temperature and nitrate have an inverse sigmoidal relationship that can be reconstructed using a locally weighted scatterplot smoothing nonparametric regression with $f = 0.1$ (where the f parameter balances regression smoothness versus accuracy; see Figures A1a and A1b). The locally weighted scatterplot smoothing regression equation can then be applied to the mooring temperature time series to reconstruct nitrate for the deployment period. To confirm the accuracy of this method, we calculated temperature-reconstructed nitrate time series for the entire duration of each mooring and compared those time series to corresponding CalCOFI nitrate values and measured nitrate from bottle samples obtained during mooring deployment or recovery (see Figures A1c and A1d for CCE2 reconstruction; bottle samples not shown; rho $= 0.77$, $p < 0.01$).

Chlorophyll-*a* fluorescence data undergo a three-step quality control process to calculate SFUs (cf. Powell & Ohman, 2015). First, a baseline correction is applied to the raw data as described for nitrate. Second, predeployment and post-deployment laboratory calibrations are used to calculate the average slope between fluorometer readings and known fluorescence values of laboratory-prepared chlorophyll-*a* standards. Laboratory calibrations consist of the following steps: (1) Two sets of chlorophyll-*a* standards are prepared (12 standards from pure chlorophyll-*a* extracted from *Anacystis nidulans* algae [Sigma-Aldrich C6144] in 90% acetone, in concentrations ranging from 0.0001 to 0.5 μg/L chlorophyll, and five standards from seawater collected 1 hr before dawn and diluted to: 100%, 50%, 25%, 12.5%, and 0% raw seawater, with filtered seawater filling the remaining percentage). (2) For each concentration, three replicate fluorometer voltage readings are taken and averaged to get final voltage. The third step involves aligning the time series of voltage reading and measured chlorophyll values by scaling them on separate y axes and then calculating the ratio of max measured Chl-*a*/max voltage. The daily-averaged voltage time series is then multiplied by this ratio to get the SFU time series.

Appendix B: Aragonite Saturation Calculations

We used two methods to calculate aragonite saturation at CCE2 16 m and CCE1 40 m (Method 1: pH-/total alkalinity-derived; Method 2: temperature-O_2 proxy relationship; see section 2.4 in main text for full explanation of calculations). We correlated the time series for both methods at CCE2 16 m to determine how closely their estimations matched. The correlation was significant (rho = 0.90, $p < 0.01$; not shown), indicating that the two methods produced comparable estimations.

Appendix C: Temperature Anomaly Start/End Dates

We determined start and end dates of the Warm Anomaly and El Niño based on periods of continuous positive temperature anomalies with no negative interruptions at the near-surface sensors (CCE1 at 19 m, CCE2

at 16 m). The one exception was the CCE1 Warm Anomaly start date, for which we used the CCE1 40-m data. A large positive temperature anomaly occurred at CCE1 at 40 m in June 2014 and was of the same magnitude as subsequent temperature anomalies, so we included that period in the scope of the Warm Anomaly, although we based all other CCE1 dates on the 19-m time series. Although moderate positive temperature and negative nitrate and Chl-*a* anomalies occurred intermittently at both moorings in spring 2014, we demarcated 15 June 2014 as the start of the 2014–2015 Warm Anomaly because that date was the beginning of continuous positive temperature anomalies that lasted through February 2015 and because the temperature anomalies that appeared in June 2014 were significantly greater than temperature anomalies in spring 2014. The mean temperature anomaly at CCE2 during our 2014–2015 Warm Anomaly period was 1.57 °C, compared to anomalies of <1.1 °C in spring 2014 with only one 10-day period of 1.4 °C. The mean Warm Anomaly temperature at CCE1 40 m was 1.44 °C, while anomalies in spring 2014 never rose above 0.6 °C. The CCE1 time series at 19 m never reached negative anomalies between the start of the Warm Anomaly in 2014 and the end of El Niño in 2016. Instead, we used a threshold of anomalies less than +1 °C in spring 2015 to demarcate the end of the Warm Anomaly and beginning of El Niño.

We demarcated the Warm Anomaly start date as 15 June 2014 at both CCE2 and CCE1 and the end dates as 11 May 2015 at CCE2 and 6 April 2015 at CCE1. We demarcated the El Niño start dates as 20 July 2015 at CCE2 and 16 May 2015 at CCE1 and the end dates as 27 March 2016 at CCE2 and 11 May 2016 at CCE1.

Acknowledgments
We thank all contributors to the CCE moorings program, particularly the engineers and technicians in the Send and Martz Labs, C.L. Sabine (University of Hawaii), and the captains and crews of the ships used to deploy the moorings. We thank C. Lowcher, J. Sevadjian, and T. Wirth for data processing and quality control, L. Sala and past managers of the Pelagic Invertebrate Collection for enumerations of CalCOFI zooplankton samples and discussion about mollusc population changes, and P. Franks for discussion. This work was supported by the NOAA Ocean Observing and Monitoring Division and Ocean Acidification Program (NA15OAR4320071), NSF OCE-1614359 and OCE-1637632 to the CCE-LTER site, an NSF Graduate Research Fellowship to L. Lilly, and in-kind support from NOAA NMFS and SWFSC. R. Feely and A. Sutton were supported by the Office of Oceanic and Atmospheric Research of NOAA, U.S. Department of Commerce, including resources from the Ocean Observing and Monitoring Division of the Climate Program Office (fund reference 100007298), and the Ocean Acidification Program. This is PMEL contribution 4962. CCE moorings are part of the international OceanSITES program. Quality controlled data are available online (ftp://data.ndbc.noaa.gov/data/oceansites/DATA/CCE1/and ftp://data.ndbc.noaa.gov/data/oceansites/DATA/CCE2/). Surface ocean pCO_2 data are available online (https://www.nodc.noaa.gov/ocads/oceans/time_series_moorings.html). The altimetry data study has been conducted using E.U. Copernicus Marine Service Information. The authors declare no competing interests.

Appendix D: Validity of Altimetry-Derived Particle Trajectories

To assess how well the altimetry-derived particle trajectories represent reality, we compared altimetry to in situ velocity data from the CCE1 mooring as follows: For most of 2011–2016, the buoy was equipped with a downward-facing ADCP; we integrated ADCP velocities at 30-m depth forward in time for 45 overlapping time windows of 50 days each. This yielded 45 synthetic "trajectories" or progressive vector diagrams. If ocean velocities were the same at all locations at any given time, these would be identical to actual particle trajectories. The altimetry-derived surface velocities at the CCE1 location were integrated in an identical fashion. Figure D1a shows five comparisons of buoy-derived (solid lines) and altimetry-derived (dashed lines) progressive vector diagrams. The discrepancies between each pair, and their evolutions over time, are shown in Figure D1b. The distance from the CCE1 buoy to the nearshore continental rise is approximately 160 km. Figure D1b includes the 75th percentile for the ensemble (black line), which reaches 160 km after approximately 30 days of forward integration. We thus posit that the first 30 days of the majority of simulated trajectories will have an associated error less than the distance between the buoy and the nutrient-rich source region discussed in section 3.1. We used this 30-day duration as the cutoff for our confidence in the altimetry-derived trajectories.

References

Aguilera, V. M., Escribano, R., Vargas, C. A., & González, M. T. (2019). Upwelling modulation of functional traits of a dominant planktonic grazer during "warm-acid" El Niño 2015 in a year-round upwelling area of Humboldt Current. *Plos One*, *14*(1). https://doi.org/10.1371/journal.pone.0209823

Alin, S. R., Feely, R. A., Dickson, A. G., Hernandez-Ayon, J. M., Juranek, L. W., Ohman, M. D., & Goericke, R. (2012). Robust empirical relationships for estimating the carbonate system in the southern California Current System and application to CalCOFI hydrographic cruise data (2005-2011). *Journal of Geophysical Research*, *117*, C05033. https://doi.org/10.1029/2011jc007511

Bednaršek, N., Feely, R. A., Beck, M. W., Glippa, O., Kanerva, M., & Engstrom-Ost, J. (2018). El Nino-related thermal stress coupled with upwelling-related ocean acidification negatively impacts cellular to population-level responses in pteropods along the California Current System with implications for increased bioenergetic costs. *Frontiers in Marine Science*, *5*. https://doi.org/10.3389/fmars.2018.00486

Bednaršek, N., Feely, R. A., Reum, J. C. P., Peterson, B., Menkel, J., Alin, S. R., & Hales, B. (2014). Limacina helicina shell dissolution as an indicator of declining habitat suitability owing to ocean acidification in the California Current Ecosystem. *Proceedings of the Royal Society B*, *281*(1785). https://doi.org/10.1098/rspb.2014.0123

Bednaršek, N., Feely, R. A., Tolimieri, N., Hermann, A. J., Siedlecki, S. A., Waldbusser, G. G., et al. (2017). Exposure history determines pteropod vulnerability to ocean acidification along the US West Coast. *Scientific Reports*, *7*(1), 4526. https://doi.org/10.1038/s41598-017-03934-z

Bednaršek, N., Harvey, C. J., Kaplan, I. C., Feely, R. A., & Mozina, J. (2016). Pteropods on the edge: Cumulative effects of ocean acidification, warming, and deoxygenation. *Progress in Oceanography*, *145*, 1–24. https://doi.org/10.1016/j.pocean.2016.04.002

Bjorkstedt, E. P., Bograd, S. J., Sydeman, W. J., Thompson, S. A., Goericke, R., Durazo, R., et al. (2012). State of the California Current 2011–2012: Ecosystems respond to local forcing as La Niña wavers and wanes. *Reports of California Cooperative Oceanic Fisheries Investigations*, *53*, 41–76.

Bograd, S. J., Checkley, D. A., & Wooster, W. S. (2003). CalCOFI: A half century of physical, chemical, and biological research in the California Current System. *Deep-Sea Research Part Ii-Topical Studies in Oceanography*, *50*(14-16), 2349–2353. https://doi.org/10.1016/S0967-0645(03)00122-X

Bond, N. A., Cronin, M. F., Freeland, H., & Mantua, N. (2015). Causes and impacts of the 2014 warm anomaly in the NE Pacific. *Geophysical Research Letters*, *42*, 3414–3420. https://doi.org/10.1002/2015gl063306

Bresnahan, P. J. Jr., Martz, T. R., Takeshita, Y., Johnson, K. S., & LaShomb, M. (2014). Best practices for autonomous measurement of seawater pH with the Honeywell Durafet. *Methods in Oceanography*, *9*, 44–60. https://doi.org/10.1016/j.mio.2014.08.003

Cai, W., Borlace, S., Lengaigne, M., van Rensch, P., Collins, M., Vecchi, G., et al. (2014). Increasing frequency of extreme El Nino events due to greenhouse warming. *Nature Climate Change*, *4*(2), 111–116. https://doi.org/10.1038/Nclimate2100

Carr, M. E., & Kearns, E. J. (2003). Production regimes in four Eastern Boundary Current systems. *Deep-Sea Research Part Ii-Topical Studies in Oceanography*, *50*(22-26), 3199–3221. https://doi.org/10.1016/j.dsr2.2003.07.015

Chao, Y., Farrara, J. D., Bjorkstedt, E., Chai, F., Chavez, F., Rudnick, D. L., et al. (2017). The origins of the anomalous warming in the California coastal ocean and San Francisco Bay during 2014-2016. *Journal of Geophysical Research: Oceans*, *122*, 7537–7557. https://doi.org/10.1002/2017jc013120

Chavez, F. P. (1996). Forcing and biological impact of onset of the 1992 El Niño in central California. *Geophysical Research Letters*, *23*(3), 265–268. https://doi.org/10.1029/96GL00017

Chavez, F. P., Pennington, J. T., Castro, C. G., Ryan, J. P., Michisaki, R. P., Schlining, B., et al. (2002). Biological and chemical consequences of the 1997-1998 El Nino in central California waters. *Progress in Oceanography*, *54*(1-4), 205–232. https://doi.org/10.1016/S0079-6611(02)00050-2

Chavez, F. P., Pennington, J. T., Herlien, R., Jannasch, H., Thurmond, G., & Friederich, G. E. (1997). Moorings and drifters for real-time interdisciplinary oceanography. *Journal of Atmospheric and Oceanic Technology*, *14*(5), 1199–1211. https://doi.org/10.1175/1520-0426(1997)014<1199:MADFRT>2.0.CO;2

Chelton, D. B. (1982). Large-scale response of the California Current to forcing by the wind stress curl. *CalCOFI Report*, *23*, 30–148.

Chelton, D. B., Bernal, P. A., & Mcgowan, J. A. (1982). Large-scale interannual physical and biological interaction in the California Current. *Journal of Marine Research*, *40*(4), 1095–1125.

Cushing, D. H. (1971). Upwelling and production on fish. *Advances in Marine Biology*, *9*. https://doi.org/10.1016/S0065-2881(08)60344-2

Di Lorenzo, E. (2003). Seasonal dynamics of the surface circulation in the Southern California Current System. *Deep Sea Research Part II: Topical Studies in Oceanography*, *50*(14-16), 2371–2388. https://doi.org/10.1016/S0967-0645(03)00125-5

Di Lorenzo, E., & Mantua, N. (2016). Multi-year persistence of the 2014/15 North Pacific marine heatwave. *Nature Climate Change*, *6*(11), 1042–1047. https://doi.org/10.1038/nclimate3082

Di Lorenzo, E., Schneider, N., Cobb, K. M., Franks, P. J. S., Chhak, K., Miller, A. J., et al. (2008). North Pacific Gyre Oscillation links ocean climate and ecosystem change. *Geophysical Research Letters*, *35*, L08607. https://doi.org/10.1029/2007GL032838

Feely, R. A., Alin, S. R., Carter, B., Bednaršek, N., Hales, B., Chan, F., et al. (2016). Chemical and biological impacts of ocean acidification along the west coast of North America. *Estuarine Coastal and Shelf Science*, *183*, 260–270. https://doi.org/10.1016/j.ecss.2016.08.043

Feely, R. A., Okazaki, R. R., Cai, W. J., Bednarsek, N., Alin, S. R., Byrne, R. H., & Fassbender, A. (2018). The combined effects of acidification and hypoxia on pH and aragonite saturation in the coastal waters of the California current ecosystem and the northern Gulf of Mexico. *Continental Shelf Research*, *152*, 50–60. https://doi.org/10.1016/j.csr.2017.11.002

Feely, R. A., Sabine, C. L., Hernandez-Ayon, J. M., Ianson, D., & Hales, B. (2008). Evidence for upwelling of corrosive "acidified" water onto the continental shelf. *Science*, *320*(5882), 1490–1492. https://doi.org/10.1126/science.1155676

Fiedler, P. C. (1984). Satellite-Observations of the 1982-1983 El-Nino along the United-States Pacific Coast. *Science*, *224*(4654), 1251–1254. https://doi.org/10.1126/science.224.4654.1251

Fiedler, P. C., & Mantua, N. J. (2017). How are warm and cool years in the California Current related to ENSO? *Journal of Geophysical Research: Oceans*, *122*, 5936–5951. https://doi.org/10.1002/2017jc013094

Fisher, J. L., Peterson, W. T., & Rykaczewski, R. R. (2015). The impact of El Niño events on the pelagic food chain in the northern California Current. *Global Change Biology*, *21*(12), 4401–4414. https://doi.org/10.1111/gcb.13054

Flament, P. (2002). A state variable for characterizing water masses and their diffusive stability: Spiciness. *Progress in Oceanography*, *54*(1-4), 493–501. https://doi.org/10.1016/S0079-6611(02)00065-4

Frischknecht, M., Munnich, M., & Gruber, N. (2017). Local atmospheric forcing driving an unexpected California Current System response during the 2015–2016 El Nino. *Geophysical Research Letters*, *44*, 304–311. https://doi.org/10.1002/2016gl071316

Frischknecht, M., Münnich, M., & Gruber, N. (2018). Origin, transformation, and fate: The three-dimensional biological pump in the California Current System. *Journal of Geophysical Research: Oceans*, *123*, 7939–7962. https://doi.org/10.1029/2018JC013934

Gentemann, C. L., Fewings, M. R., & Garcia-Reyes, M. (2017). Satellite sea surface temperatures along the West Coast of the United States during the 2014–2016 northeast Pacific marine heat wave. *Geophysical Research Letters*, *44*, 312–319. https://doi.org/10.1002/2016gl071039

Gruber, N., Hauri, C., Lachkar, Z., Loher, D., Frolicher, T. L., & Plattner, G. K. (2012). Rapid progression of ocean acidification in the California Current System. *Science*, *337*(6091), 220–223. https://doi.org/10.1126/science.1216773

Hartman, S. E., Larkin, K. E., Lampitt, R. S., Lankhorst, M., & Hydes, D. J. (2010). Seasonal and inter-annual biogeochemical variations in the Porcupine Abyssal Plain 2003-2005 associated with winter mixing and surface circulation. *Deep-Sea Research Part Ii-Topical Studies in Oceanography*, *57*(15), 1303–1312. https://doi.org/10.1016/j.dsr2.2010.01.007

Hauri, C., Gruber, N., McDonnell, A. M. P., & Vogt, M. (2013). The intensity, duration, and severity of low aragonite saturation state events on the California continental shelf. *Geophysical Research Letters*, *40*, 3424–3428. https://doi.org/10.1002/grl.50618

Hauri, C., Gruber, N., Vogt, M., Doney, S. C., Feely, R. A., Lachkar, Z., et al. (2013). Spatiotemporal variability and long-term trends of ocean acidification in the California Current System. *Biogeosciences*, *10*(1), 193–216. https://doi.org/10.5194/bg-10-193-2013

Hu, S. N., & Fedorov, A. V. (2016). Exceptionally strong easterly wind burst stalling El Nino of 2014. *Proceedings of the National Academy of Sciences of the United States of America*, *113*(8), 2005–2010. https://doi.org/10.1073/pnas.1514182113

Jacox, M. G., Hazen, E. L., Zaba, K. D., Rudnick, D. L., Edwards, C. A., Moore, A. M., & Bograd, S. J. (2016). Impacts of the 2015–2016 El Nino on the California Current System: Early assessment and comparison to past events. *Geophysical Research Letters*, *43*, 7072–7080. https://doi.org/10.1002/2016gl069716

Janssen, A. W., Bush, S. L., & Bednaršek, N. (2019). The shelled pteropods of the northeast Pacific Ocean (Mollusca: Heterobranchia, Pteropoda). *Zoosymposia*, *13*(1), 305–346. https://doi.org/10.11646/zoosymposia.13.1.22

Kahru, M., & Mitchell, B. G. (2000). Influence of the 1997–98 El Nino on the surface chlorophyll in the California Current. *Geophysical Research Letters*, *27*(18), 2937–2940. https://doi.org/10.1029/2000gl011486

Keiper, C. A., Ainley, D. G., Allen, S. G., & Harvey, J. T. (2005). Marine mammal occurrence and ocean climate off central California, 1986 to 1994 and 1997 to 1999. *Marine Ecology Progress Series*, *289*, 285–306. https://doi.org/10.3354/meps289285

Lavaniegos, B. E., Jimenez-Perez, L. C., & Gaxiola-Castro, G. (2002). Plankton response to El Nino 1997–1998 and La Nina 1999 in the southern region of the California Current. *Progress in Oceanography*, *54*(1-4), 33–58. https://doi.org/10.1016/S0079-6611(02)00042-3

Lavaniegos, B. E., & Ohman, M. D. (2007). Coherence of long-term variations of zooplankton in two sectors of the California Current System. *Progress in Oceanography*, *75*(1), 42–69. https://doi.org/10.1016/j.pocean.2007.07.002

Lee, D. E., Nur, N., & Sydeman, W. J. (2007). Climate and demography of the planktivorous Cassin's auklet Ptychoramphus aleuticus off northern California: Implications for population change. *Journal of Animal Ecology*, *76*(2), 337–347. https://doi.org/10.1111/j.1365-2656.2007.01198.x

Lee, T., & McPhaden, M. J. (2010). Increasing intensity of El Nino in the central-equatorial Pacific. *Geophysical Research Letters*, *37*, L14603. https://doi.org/10.1029/2010gl044007

Leinweber, A., & Gruber, N. (2013). Variability and trends of ocean acidification in the Southern California Current System: A time series from Santa Monica Bay. *Journal of Geophysical Research: Oceans*, *118*, 3622–3633. https://doi.org/10.1002/jgrc.20259

Li, J. Y., Liu, B. Q., Li, J. D., & Mao, J. Y. (2015). A comparative study on the dominant factors responsible for the weaker-than-expected El Nino Event in 2014. *Advances in Atmospheric Sciences*, *32*(10), 1381–1390. https://doi.org/10.1007/s00376-015-4269-6

Lilly, L. E., & Ohman, M. D. (2018). CCE IV: El Niño-related zooplankton variability in the southern California Current System. *Deep-Sea Research Part I: Oceanographic Research Papers*, *140*, 36–51.

Locarnini, R. A., Mishonov, A. V., Antonov, J. I., Boyer, T. P., Garcia, H. E., Baranova, O. K., et al. (2013). In E. S. Levitus, & T. E. A. Mishonov (Eds.), *World Ocean Atlas 2013, Volume 1: Temperature*, NOAA Atlas NESDIS (Vol. *73*, p. 40).

Lynn, R. J., & Bograd, S. J. (2002). Dynamic evolution of the 1997–1999 El Nino–La Nina cycle in the southern California Current System. *Progress in Oceanography*, *54*(1-4), 59–75.

Lynn, R. J., & Simpson, J. J. (1987). The California Current System—The seasonal variability of its physical characteristics. *Journal of Geophysical Research*, *92*(C12). https://doi.org/10.1029/JC092iC12p12947

Mantua, N. J., Hare, S. R., Zhang, Y., Wallace, J. M., & Francis, R. C. (1997). A Pacific interdecadal climate oscillation with impacts on salmon production. *Bulletin of the American Meteorological Society*, *78*(6), 1069–1079. https://doi.org/10.1175/1520-0477(1997)078<1069:Apicow>2.0.Co;2

McCabe, R. M., Hickey, B. M., Kudela, R. M., Lefebvre, K. A., Adams, N. G., Bill, B. D., et al. (2016). An unprecedented coastwide toxic algal bloom linked to anomalous ocean conditions. *Geophysical Research Letters*, *43*, 10366–10376. https://doi.org/10.1002/2016GL070023

McGowan, J. A. (1967). Distributional atlas of pelagic molluscs in the California Current region. *CalCOFI Atlas*, *6*.

McLaughlin, K., Nezlin, N. P., Weisberg, S. B., Dickson, A. G., Booth, J. A. T., Cash, C. L., et al. (2018). Seasonal patterns in aragonite saturation state on the southern California continental shelf. *Continental Shelf Research.*, *167*, 77–86. https://doi.org/10.1016/j.csr.2018.07.009

Osborne, E. B., Thunell, R. C., Marshall, B. J., Holm, J. A., Tappa, E. J., Benitez-Nelson, C., et al. (2016). Calcification of the planktonic foraminifera Globigerina bulloides and carbonate ion concentration: Results from the Santa Barbara Basin. *Paleoceanography*, *31*, 1083–1102. https://doi.org/10.1002/2016pa002933

Pennington, J. T., & Chavez, F. P. (2000). Seasonal fluctuations of temperature, salinity, nitrate, chlorophyll and primary production at station H3/M1 over 1989–1996 in Monterey Bay, California. *Deep Sea Research Part II: Topical Studies in Oceanography*, *47*(5-6), 947–973. https://doi.org/10.1016/S0967-0645(99)00132-0

Peterson, W. T., Fisher, J. L., Strub, P. T., Du, X., Risien, C., Peterson, J., & Shaw, C. T. (2017). The pelagic ecosystem in the Northern California Current off Oregon during the 2014–2016 warm anomalies within the context of the past 20 years. *Journal of Geophysical Research: Oceans*, *122*, 7267–7290. https://doi.org/10.1002/2017JC012952

Peterson, W. T., Robert, M. & Bond, N. A. (2015). The warm blob continues to dominate the ecosystem of the northern California current. Retrieved from PICES Press Vol. 23, No. 2: https://search.proquest.com/docview/1705538895/fulltext/BD3F90E0734A43E3PQ/1?accountid=14524

Pickett, M. H., & Paduan, J. D. (2003). Ekman transport and pumping in the California Current based on the U.S. Navy's high-resolution atmospheric model (COAMPS). *Journal of Geophysical Research*, *108*(C10), 3327. https://doi.org/10.1029/2003jc001902

Powell, J. R., & Ohman, M. D. (2015). Covariability of zooplankton gradients with glider-detected density fronts in the Southern California Current System. *Deep-Sea Research Part Ii-Topical Studies in Oceanography*, *112*, 79–90. https://doi.org/10.1016/j.dsr2.2014.04.002

Rebstock, G. A. (2001). Long-term stability of species composition in calanoid copepods off southern California. *Marine Ecology Progress Series*, *215*, 213–224. https://doi.org/10.3354/meps215213

Robinson, C. J. (2016). Evolution of the 2014–2015 sea surface temperature warming in the central west coast of Baja California, Mexico, recorded by remote sensing. *Geophysical Research Letters*, *43*, 7066–7071. https://doi.org/10.1002/2016GL069356

Rudnick, D. L., Zaba, K. D., Todd, R. E., & Davis, R. E. (2017). A climatology of the California Current System from a network of underwater gliders. *Progress in Oceanography*, *154*, 64–106. https://doi.org/10.1016/j.pocean.2017.03.002

Ryan, J. P., Kudela, R. M., Birch, J. M., Blum, M., Bowers, H. A., Chavez, F. P., et al. (2017). Causality of an extreme harmful algal bloom in Monterey Bay, California, during the 2014–2016 northeast Pacific warm anomaly. *Geophysical Research Letters*, *44*, 5571–5579. https://doi.org/10.1002/2017GL072637

Rykaczewski, R. R., & Checkley, D. M. (2008). Influence of ocean winds on the pelagic ecosystem in upwelling regions. *Proceedings of the National Academy of Sciences of the United States of America*, *105*(6), 1965–1970. https://doi.org/10.1073/pnas.0711777105

Sakamoto, C. M., Johnson, K. S., Coletti, L. J., Maurer, T. L., Massion, G., Pennington, J. T., et al. (2017). Hourly in situ nitrate on a coastal mooring: A 15-year record and insights into new production. *Oceanography*, *30*(4), 114–127. https://doi.org/10.5670/oceanog.2017.428

Simpson, J. J. (1984). El-Nino-induced onshore transport in the California Current during 1982–1983. *Geophysical Research Letters*, *11*(3), 241–242.

Sutton, A. J., Sabine, C. L., Feely, R. A., Cai, W. J., Cronin, M. F., McPhaden, M. J., et al. (2016). Using present-day observations to detect when anthropogenic change forces surface ocean carbonate chemistry outside preindustrial bounds. *Biogeosciences*, *13*(17), 5065–5083. https://doi.org/10.5194/bg-13-5065-2016

Sutton, A. J., Sabine, C. L., Maenner-Jones, S., Lawrence-Slavas, N., Meinig, C., Feely, R. A., et al. (2014). A high-frequency atmospheric and seawater pCO_2 data set from 14 open-ocean sites using a moored autonomous system. *Earth System Science Data*, *6*(2), 353–366. https://doi.org/10.5194/essd-6-353-2014

Thayer, J. A., & Sydeman, W. J. (2007). Spatio-temporal variability in prey harvest and reproductive ecology of a piscivorous seabird, Cerorhinca monocerata, in an upwelling system. *Marine Ecology Progress Series*, *329*, 253–265. https://doi.org/10.3354/meps329253

Todd, R. E., Rudnick, D. L., Davis, R. E., & Ohman, M. D. (2011). Underwater gliders reveal rapid arrival of El Nino effects off California's coast. *Geophysical Research Letters*, *38*, L03609. https://doi.org/10.1029/2010GL046376

Van Heuven, S., Pierrot, D., Rae, J., Lewis, E. & Wallace, D. (2011). MATLAB program developed for CO2 system calculations. Oak Ridge, Tennessee: Carbon Dioxide Information Analysis Center, Oak Ridge National Laboratory, US Department of Energy.

Wells, B. K., Schroeder, I. D., Santora, J. A., Hazen, E. L., Bograd, S. J., Bjorkstedt, E. P., et al. (2013). State of the California Current 2012–13: No such thing as an "average" year. *California Cooperative Oceanic Fisheries Investigations Reports*, *54*(37-71).

Zaba, K. D., & Rudnick, D. L. (2016). The 2014-2015 warming anomaly in the Southern California Current System observed by underwater gliders. *Geophysical Research Letters*, *43*, 1241–1248. https://doi.org/10.1002/2015gl067550

Zweng, M. M., Reagan, J. R., Antonov, J. I., Locarnini, R. A., Mishonov, A. V., Boyer, T. P., et al. (2013). In E. S. Levitus, & T. E. A. Mishonov (Eds.), *World Ocean Atlas 2013, Volume 2: Salinity*, NOAA Atlas NESDIS (Vol. *74*, p. 39).

Journal of Geophysical Research: Oceans

Supporting Information for

Biogeochemical anomalies at two southern California Current System moorings during the 2014-16 Warm Anomaly-El Niño sequence

Laura E. Lilly[1,2]*, Uwe Send[2,3], Matthias Lankhorst[3], Todd R. Martz[2,4], Richard A. Feely[5], Adrienne J. Sutton[5], and Mark D. Ohman[1,2]

[1]Integrative Oceanography Division, Scripps Institution of Oceanography, University of California, San Diego, La Jolla, CA, USA

[2]California Current Ecosystem Long-Term Ecological Research site, Scripps Institution of Oceanography, University of California, San Diego, La Jolla, CA, USA

[3]Climate, Atmospheric Sciences, and Physical Oceanography, Scripps Institution of Oceanography, University of California, San Diego, La Jolla, CA, USA

[4]Geosciences Research Division, Scripps Institution of Oceanography, University of California, San Diego, La Jolla, CA, USA

[5]NOAA Pacific Marine Environmental Laboratory, Seattle, WA, USA

*Corresponding author: Laura Lilly (l1lilly@ucsd.edu)

Contents of this file

Introduction

This supporting figure provides additional resolution beyond figure 5 in the main text. In particular: 1) it shows particle tracks by individual year, which allows the reader to more clearly compare years, and 2) it color-codes each year for within-year seasonality, which allows the reader to track the specific timing of particle movements.

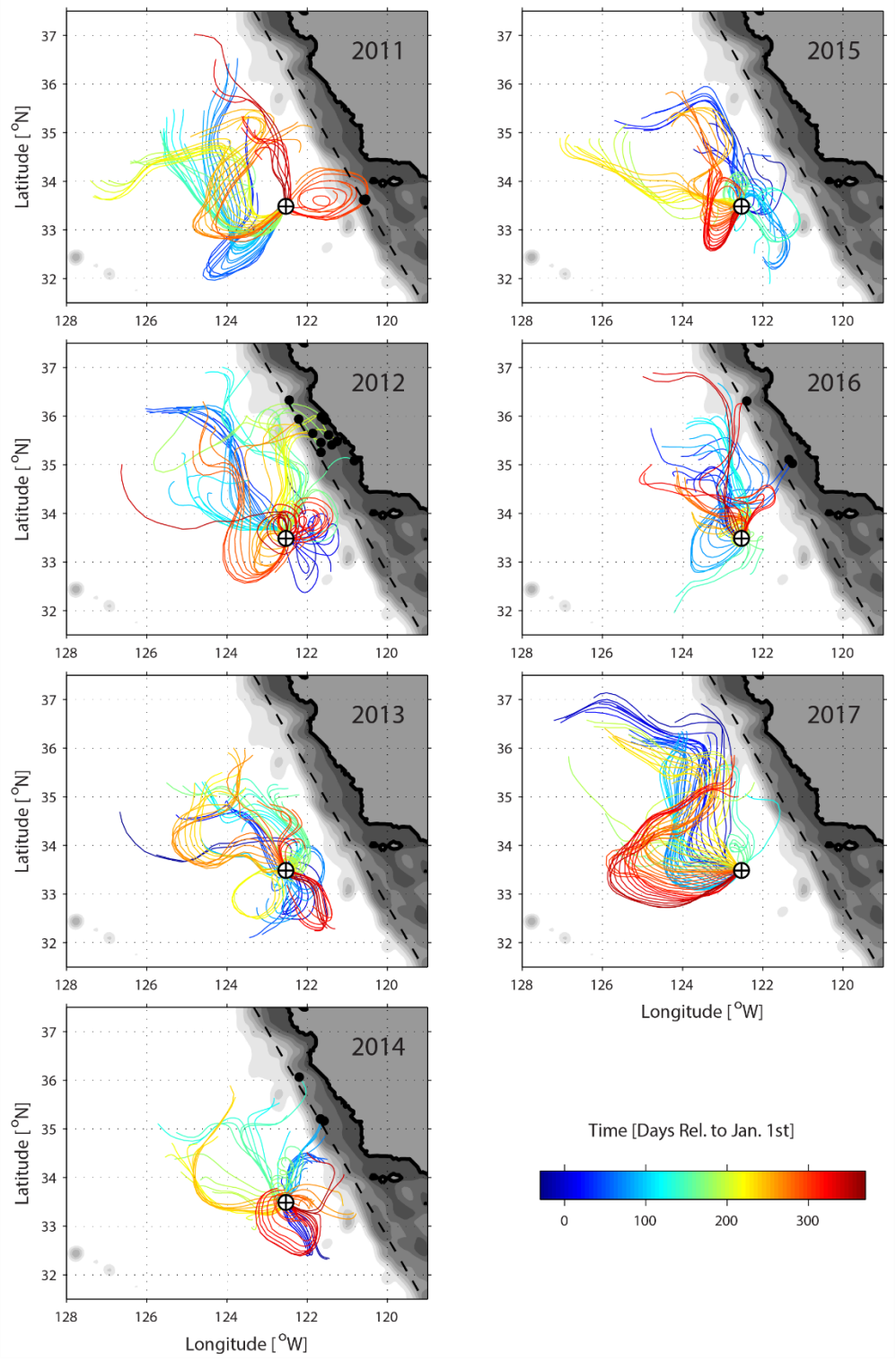

Figure S1. As in figure 5c, but with particle tracks separated by individual year. Color scale indicates day numbers within each year.